Photonuclear production of nuclear isomers using bremsstrahlung induced by laser-wakefield electrons*

Hao-Yang Lan,[1] Di Wu,[1] Jia-Xin Liu,[1] Jian-Yao Zhang,[1] Huan-Gang Lu,[1] Jian-Feng Lv,[1] Xue-Zhi Wu,[1] Wen Luo,[2] and Xue-Qing Yan[1,†]

[1]*State Key Laboratory of Nuclear Physics and Technology, and Key Laboratory of HEDP of the Ministry of Education, CAPT, Peking University, Beijing 100871, China*
[2]*School of Nuclear Science and Technology, University of South China, Hengyang 421001, China*

In this study, we theoretically investigate the feasibility of using laser-wakefield accelerated (LWFA) electrons for the photonuclear measurement of nuclear isomers according to the characteristics of the electrons obtained from LWFA experiments conducted at the Compact Laser Plasma Accelerator (CLAPA) laboratory. The experiments at the CLAPA show that a stable electron beam with an energy of 78–135 MeV and a charge of 300-600 pC can be obtained. The bremsstrahlung spectra were simulated using Geant4, which suggests that a bremsstrahlung source with a peak intensity of 10^{19} photons/s can be generated. Theoretical calculations of isomer production cross-sections from the photonuclear reactions on six target nuclei, ^{197}Au, ^{180}Hf, ^{159}Tb, ^{115}In, ^{103}Rh, and ^{90}Zr were performed and compared with the available experimental data in EXFOR, which suggest that further experiments are required for a series of photonuclear reaction channels. Flux-averaged cross sections and isomer ratios (IR) resulting from such bremsstrahlung sources are theoretically deduced. The results suggest that IR measurements can be used to constrain nuclear components, such as γ strength function and optical model potential. In addition, the detection of the decay characteristics was evaluated with Geant4 simulations. The use of the LWFA electron beam and its bremsstrahlung for photonuclear studies involving nuclear isomers is anticipated.

Keywords: Photonuclear reactions; Laser plasma acceleration; Flux-averaged isomer ratio

I. INTRODUCTION

Since the theoretical prediction by Soddy [1] in 1917 and the first experimental observation by Hahn [2] in 1921, nuclear isomers have received intensive attention from the perspective of fundamental research and applicational development [3, 4]. In particular, the effective population and manipulation of nuclear isomers has been an active topic in recent years, driven by the prospect of utilizing their intrinsic or depleted decays for the development of nuclear clocks, nuclear batteries, and gamma lasers [5–9]. Moreover, the exploration of nuclei with isomeric states in nuclear astrophysics allows us to determine how they affect the creation of elements in the universe and how they eventually contribute to the makeup of life in our cosmos [10].

In recent decades, the worldwide development of high-intensity and high-repetition-rate laser systems has opened up new research opportunities for particle acceleration [11–17] and nuclear photonics [18]. In particular, the ultra-short pulse radiation source and plasma environment generated by the interaction between the laser and target provide unique physical environments for the study of nuclear isomers. Using a table-top hundred TW laser, Feng et al. [19] demonstrated that the femtosecond pumping of ^{83m}Kr with a peak efficiency of 2.34×10^{15} s^{-1} can be achieved through the Coulomb excitation of ions with quivering electrons during the interaction between laser pulses and clusters at nearly solid densities. Wang et al. [20] proposed a novel approach to populate the nuclear clock isomer ^{229m}Th by combining laser-driven electron recollision and electronic nuclear excitation, for example, Coulomb excitation, which does not require precise knowledge of the isomeric energy. The common idea of these schemes is to make use of the dense low-energy electrons produced in laser-plasma interactions and the relatively high electronic excitation cross sections of ionized atoms in plasma. A comprehensive comparison of the possible physical processes for isomer population and manipulation, including nuclear excitation by electron capture, excitation by electron transition, electron bridge, and photoactivation, was also given in Ref. [21], which indicates that nuclear excitations assisted by electrons would be far more efficient than straightforward photon excitation. This is reasonable for isomer manipulation or triggered isomer depletion circumstances, where the target nucleus must remain unchanged, and the excitation energy required is as low as the difference between the atomic electron shells. However, this is somehow not the case when it comes to the isomer population, where the isomer can be populated without extra scruples on the disintegration of the target nucleus. Specifically, the cross-section of photonuclear reactions can be significantly enhanced by giant dipole resonances (GDR) to hundreds of millibarns above the neutron separation threshold, whereas only the narrow discrete resonance from the isolated bound states is generally mentioned in most of the discussions for photo-activation of nuclear isomers. Utilizing (γ,γ') scattering of the collective excitation mode, Pan et al. [22] have depicted the prospect of accumulating isomers of medical interest to a clinically applicable activity with an intense

* This work was supported by the National Natural Science Foundation of China (Nos. 11921006, U2230133), Beijing Outstanding Young Scientists Program, National Grand Instrument Project (No. 2019YFF01014400), National Key R&D Program of China (No. 2022YFA1603303), and Open Foundation of Key Laboratory of High Power Laser and Physics, Chinese Academy of Sciences (No. SGKF202104).
† Corresponding author, x.yan@pku.edu.cn

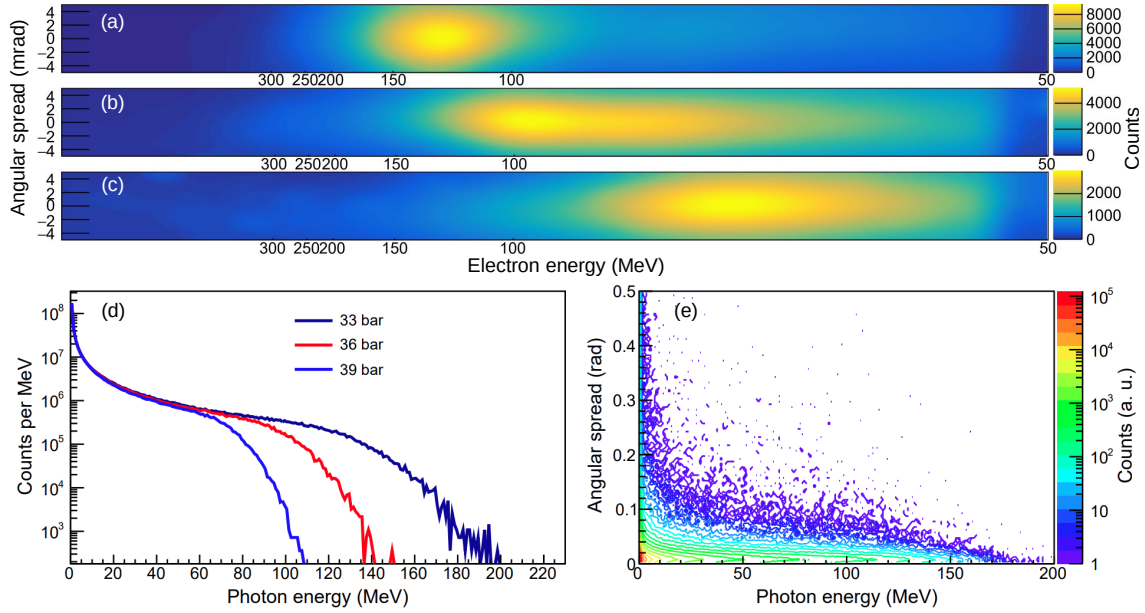

Fig. 1. (Color online) Panels (a), (b), and (c) are the exemplary LWFA electron spectra obtained from the back pressure of 33, 36, and 39 bar, respectively. (d) The bremsstrahlung energy spectrum obtained from the Geant4 simulations considering the averaged energy spectra and angular spread of 100 LWFA electron shots. (e) The correlation of bremsstrahlung energy against its angular spread for electrons at 33 bars.

monochromatic γ-ray beam. Meanwhile, quasimonochromatic high-intensity electron pulses generated by laser wakefield acceleration (LWFA) in gas jets are commonly available in high-power laser facilities, which can be converted into bremsstrahlung radiation, thus providing vast research opportunities for photonuclear studies. Although previous studies have utilized laser-driven photonuclear reactions for electron diagnosis [23], nuclear waste transmutation [24], and medical isotope production [25], little attention has been paid to nuclear isomers. Consequently, a systematic investigation is required to evaluate the potential of the isomer population by laser-driven photonuclear excitation.

In this work, we theoretically investigate the potential to accumulate nuclear isomers by laser-driven photonuclear excitation through Monte Carlo simulations based on the electron characteristics obtained from LWFA experiments. LWFA experiments at the Compact Laser Plasma Accelerator (CLAPA) laboratory of Peking University are introduced, and the conversion from electrons to bremsstrahlung is simulated with the Geant4 [26]. Then, theoretical calculations on the photonuclear cross-sections are performed. A series of nuclear isomers were selected as the calculation candidates, considering both the nuclear flow of photonuclear reactions and the availability of stable natural target nuclei. The corresponding photonuclear cross-sections for isomer generation were evaluated using TALYS [27, 28]. To verify the reliability of the TALYS inputs, a benchmark of the theoretical predictions against the available experimental data extracted from the experimental nuclear reaction database, EXFOR [29] is performed. The flux-averaged cross-sections and flux-averaged isomer ratios were deduced according to the theoretical photonuclear cross-sections and simulated bremsstrahlung spectra. Furthermore, the photonuclear cross-sections of different reaction channels were incorporated into the simulation toolkit Geant4-GENBOD [30–32] to estimate the feasibility of detecting the nuclear isomers of interest. In the simulations, the typical laser-driven electron beam parameters extracted from the experiments are considered, as well as the physical processes of the radioactive decay of various reaction residuals and energy deposition in commercially available $LaBr_3$ scintillation detectors. A comprehensive discussion is provided in the context of the production and detection of the nuclear isomers of interest.

II. LWFA ELECTRONS AND BREMSSTRAHLUNG CONVERSION AT CLAPA

We conducted experiments to accelerate electrons for bremsstrahlung generation with the 200 TW laser facility at the CLAPA of Peking University, which can deliver laser pulses with a duration of 30 fs, energy of 4 J, and repetition rate of 5 Hz. The laser beam was focused on a spot of 21×23 μm full width at maximum onto the leading edge of a 4×1 mm supersonic gas jet. The effective energy on the target was approximately 1.8 J with a laser intensity of approximately 1.5×10^{-19} W/cm^{-2}. In the interaction between the laser pulses and the mixed gas made of 5% N_2 and 95% He_2, monochromatic energetic electrons can be produced by LWFA. The electrons propagate through a thin Be window; heading out of the vacuum chamber to the magnetic spectrometer placed 100 cm downstream of the gas jet, where the

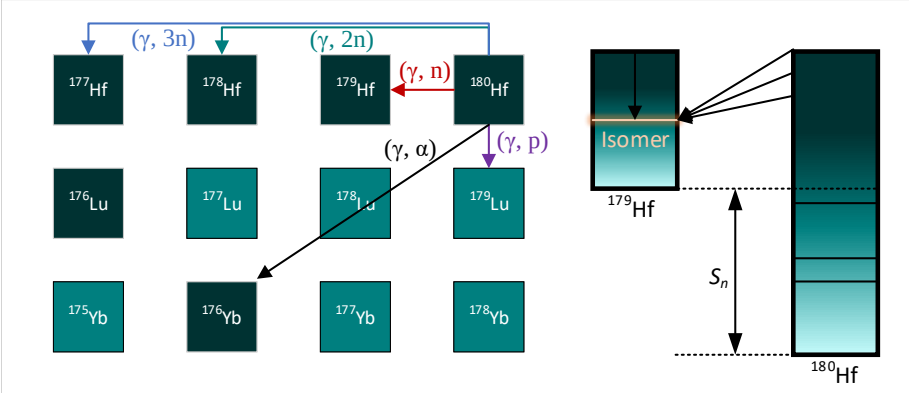

Fig. 2. (Color online) The nuclear flow of photonuclear reactions and the mechanism for isomer generation. Here S_n denotes the neutron separation energy of the target nucleus ^{180}Hf.

deflected electron signals can be diagnosed using fluorescent screens and CCD cameras. The electron charge was measured by a Turbo Integrating Current Transformer (Turbo-ICT) assembled right out of the Be window.

The back pressure of the gas jet was varied from 33 bar to 39 bar, obtaining LWFA electrons with a peak energy of 78-135 MeV. One hundred continuous shots were recorded for each gas pressure to test the stability of the accelerated electrons. The repetition rate remained at 0.25 Hz to ensure that the vacuum level of the laser-gas interaction chamber could be recovered for the LWFA. Typical electron distributions recorded by the magnetic spectrometer are shown in Fig. 1 (a)–(c). Electron energies of 78 $\pm$ 10, 103 $\pm$ 14, and 135 $\pm$ 20 MeV were obtained at 39, 36, and 33 bar, respectively. The divergence of the electrons was within 4.3 mrad and the directional stability was better than 5.2 mrad. The electron charge was measured to be 300–600 pC.

The averaged energy and divergence distributions of the electrons obtained at 39, 36, and 33 bar were incorporated into Geant4 to simulate the resulting bremsstrahlung characteristics. In the simulations, the electrons were directed to a 2-mm-thick Ta converter 1 m away from the electron generation point, inducing bremsstrahlung radiation. The electron charge was set to 300 pC, which is a conservative estimate for the number of LWFA electrons produced per shot. The bremsstrahlung photons were recorded in a plane perpendicular to the propagation direction assembled 20 cm downstream from the converter. The simulated bremsstrahlung energy distributions are shown in Fig. 1 (d). The photon intensity shows a typical decaying trend with the increase in photon energy, which can fully cover the GDR region of the selected target nuclei. The conversion efficiency from electrons to photons increases with increasing electron energy. The total photon flux can reach the order of 4.35×10^8 photons/shot, which corresponds to a peak photon flux of 1.24×10^{19} photons/s, considering a pulse duration spread of 35 ps inside the converter. The correlation between the photon energy and polar angle for the incident electrons at 33 bar is shown in Fig. 1 (e). It is shown that the angular spread of the photons tends to narrow with an increase in photon energy. The angular spread of most of the photons is within 0.4 rad. With such a photon beam with a high peak flux and ultrashort pulse duration, one can potentially measure the nuclear isomers with short half-lives produced in photonuclear reactions. Accordingly, the reaction data covering the GDR and quasi-deuteron regions were probed.

III. PRODUCTION ROUTE AND PHOTONUCLEAR CROSS-SECTIONS

A. Theory

The nuclear flow of photonuclear reactions and mechanism for isomer generation are depicted in Fig. 2. When a target nucleus is excited above the particle separation energy the excited compound subsequently decays through the emission of particles (such as neutrons, protons, and alpha particles) or photons to different energy levels of the residual, including the isomer state. At energies of 10–40 MeV the GDR resulting from the out-of-phase oscillation between the proton fluid and neutron fluid would clearly give rise to the odds of photon absorption and compound nucleus formation. At 40–130 MeV, the photon interacts with the nucleus by the quasi-deuteron mechanism (QD), where the compound nucleus decays predominantly via the emission of several nucleons, but mostly neutrons. The decay of the compound nucleus, which would lead to the population of isomers can be well described by the Hauser-Feshbach reaction model, which is based on the fundamental Bohr hypothesis that the reaction occurs by means of the intermediary formation of a compound nucleus that can reach a state of thermodynamic equilibrium. The Hauser-Feshbach model averages over many resonances in the formation of a compound nucleus and therefore can be applied if the nuclear level density (NLD) in the compound nucleus is sufficiently high at the compound formation energy, which is the excitation energy at which the compound nucleus is formed.

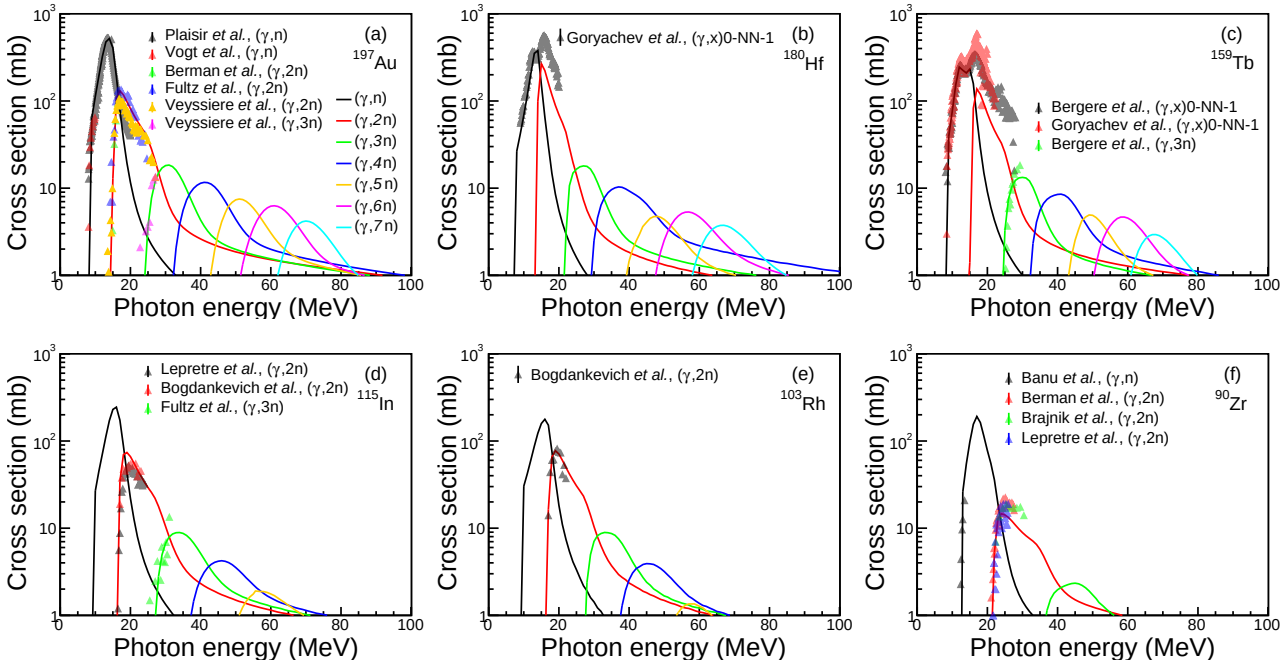

Fig. 3. (Color online) The calculated (γ,x n) cross sections for ^{197}Au, ^{180}Hf, ^{159}Tb, ^{115}In, ^{103}Rh, ^{90}Zr. The available experimental data from the EXFOR database are also shown for comparison [33–53].

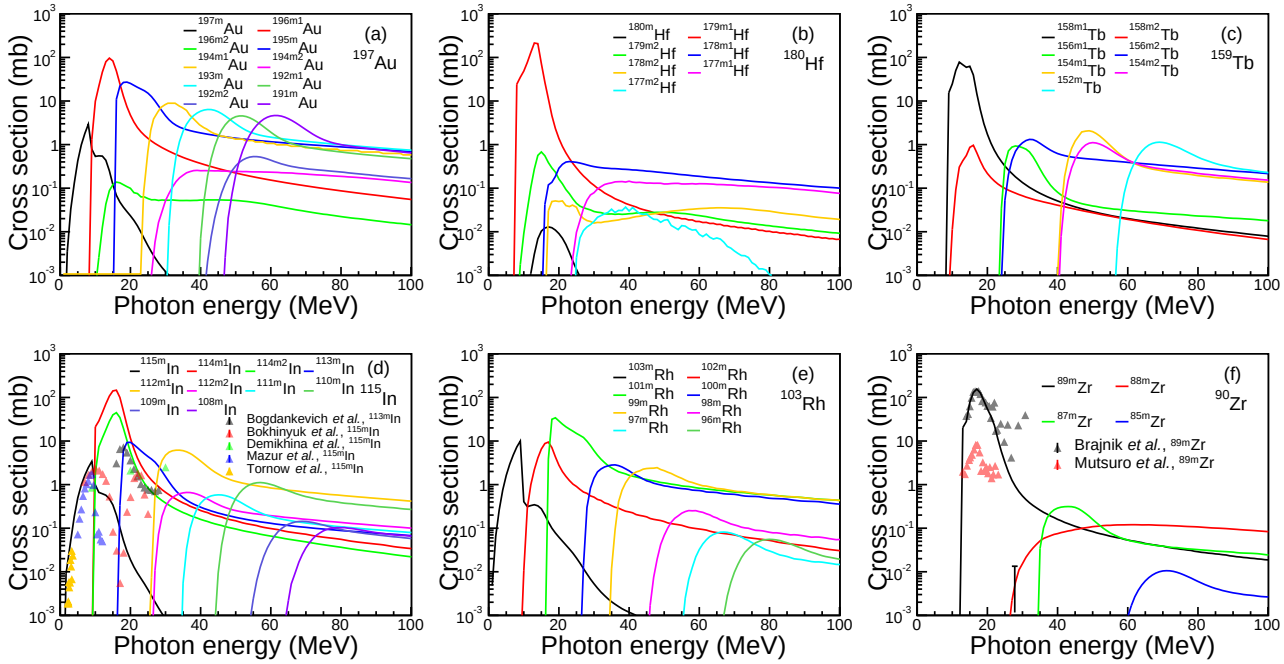

Fig. 4. (Color online) The isomer production cross sections for the six selected target nuclei. The available experimental data from the EXFOR database are also shown for comparison [54–60].

B. Verification of photonuclear cross-sections

Generally, photonuclear reactions tend to push the involved nucleus toward the down-left side of the nuclear chart. This places a clear limit on the possible populated isomers when considering the stability of the target nucleus. According to the nuclear flow of photonuclear reactions and the stability of the target nucleus, we selected a series of stable nuclides, including ^{197}Au, ^{180}Hf, ^{159}Tb, ^{115}In, ^{103}Rh, and ^{90}Zr

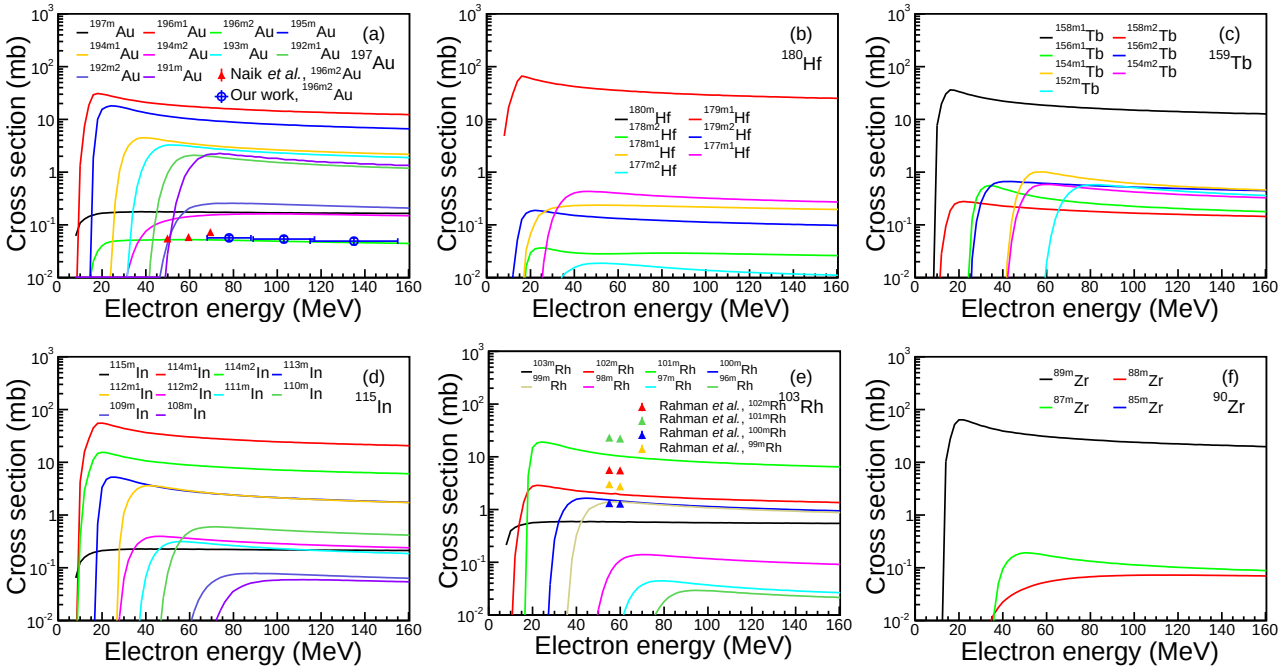

Fig. 5. (Color online) The FACS for (γ,xn) reactions for the six selected target nuclei. The available experimental data from the EXFOR database are also shown for comparison [61, 62].

as candidates for theoretical calculations of reaction cross-sections. The cross sections for typical photonuclear reactions, such as (γ, γ'), (γ, xn), (γ, p), and (γ, α), are calculated using the software package TALYS, which provides a complete description of all reaction channels and observables, and many state-of-the-art nuclear models covering all the main reaction mechanisms encountered in light-particle-induced nuclear reactions are included. The nuclear structure components used in the TALYS calculations were as follows: The nuclear masses are taken from the Atomic Mass Evaluation 2016 (AME2016) [67] whenever available, whereas the HFB-27 nuclear masses [68] are taken into account when the AME2016 mass data is not available. The discrete experimental levels compiled in the RIPL-3 library [69] and the continuum level spectrum represented by the nuclear level densities (NLDs) are both considered in the calculations. The NLDs were obtained from predictions in the Fermi gas model plus a constant temperature. The photon strength functions (SFs) obtained from the Brink-Axel Lorentzian model were used to calculate the electromagnetic transmission coefficients for the photon channel. The phenomenological optical model potentials (OMPs), i. e., the local and global parameterizations of Koning and Delaroche are employed to determine the transmission coefficient for the particle channels.

The theoretical photonuclear reaction cross-sections based on TALYS for the selected targets and their corresponding experimental data available in the EXFOR database are shown in Fig. 3. It can be seen that the (γ, n) reaction cross-section is generally dominant in the GDR region, with a maximum of hundreds of mb. As the excitation energy continues to increase, multiple emission reactions take over, whose maximum cross-section decreases with an increase in the number of emitted particles. The theoretical calculations agree with the EXFOR data, which is obtained from previous measurements using photon sources, such as (tagged) bremsstrahlung [33–39], laser-Compton γ rays [40–44], and positron annihilation in flight [45–53]. This indicates the reliability of the TALYS inputs and calculations. In addition, it is noticeable that the previous measurements have not fully covered all the photonuclear reaction channels, although the (γ,xn) reaction data for the most studied nucleus ^{197}Au are rather abundant. Future experiments are expected to provide new data for these reaction channels. The isomer production cross-sections resulting from photonuclear reactions on the six selected target nuclei are shown in Fig. 4. Isomer production from (γ, n) reactions is generally greater than that from the other reaction channels, with a maximum cross-section of hundreds of $\sim$100 mb. It is also noted that experimental isomer production cross-sections are very rare, which can be potentially measured using state-of-the-art LCS facilities [70–72] in the future.

IV. PRODUCTION YIELDS AND FLUX-AVERAGED ISOMER RATIOS

A. Isomer production yields

In bremsstrahlung-driven photonuclear measurements, isomers and their decay have long been interesting topics because they can provide constraints for nuclear structures. Under bremsstrahlung radiation, the flux average cross sections

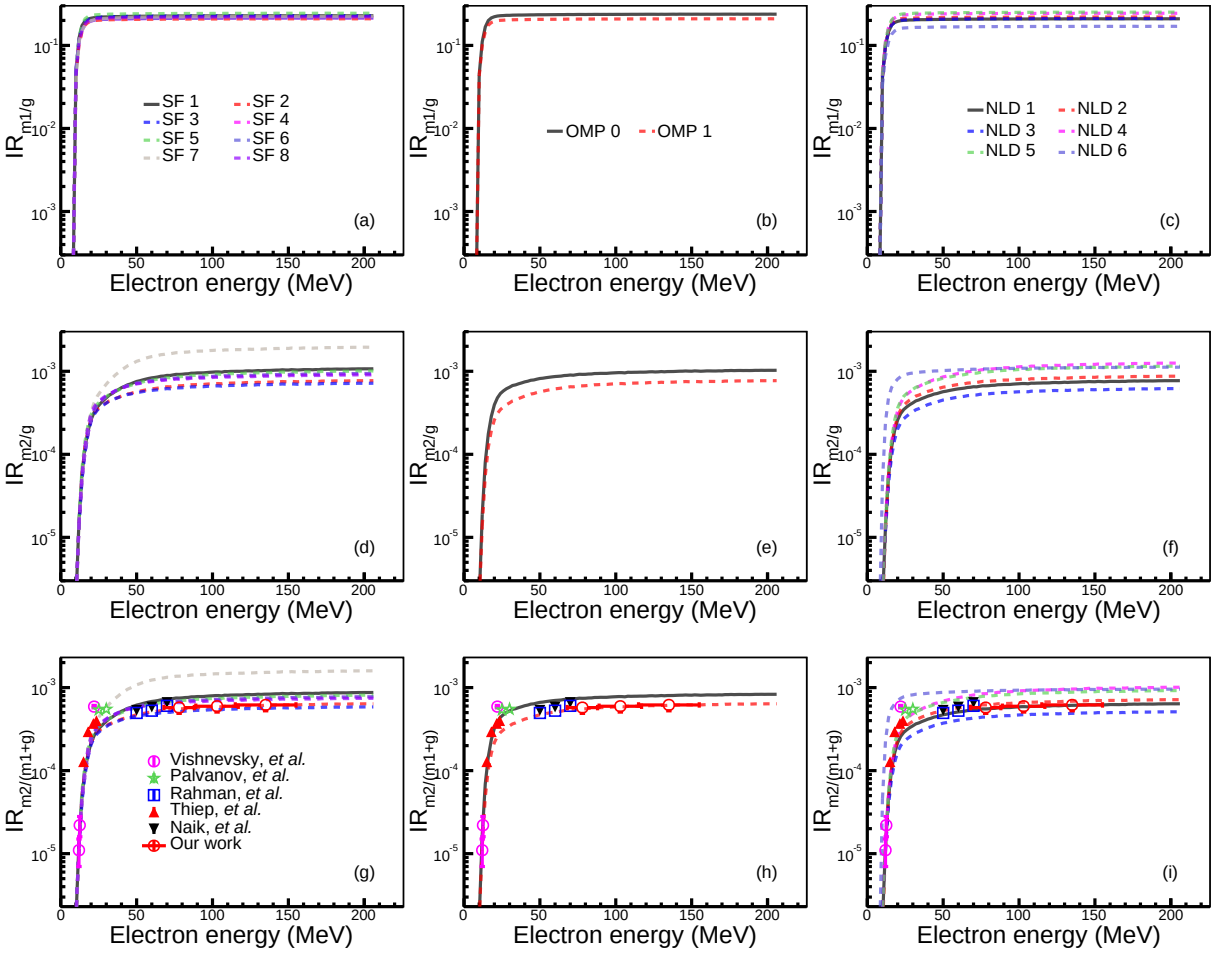

Fig. 6. (Color online) The isomer ratios of $IR_{m2/g}$ (a-c), $IR_{m2/g}$ (d-f), and $IR_{m2/(m1+g)}$ (g-i) for the ^{197}Au(γ, n) reactions calculated with six sets of eight sets of SFs, two sets of OMPs, and NLDs available in TALYS 1.9. The nuclear structure ingredients used for the calculations are indexed by numbers and described in the main text. The experimental data from EXFOR are also shown for comparison [61, 63–66].

(FACS) of a given photonuclear reaction can be given by:

$$\sigma_{\mathrm{FA}}(E_{\mathrm{e}}) = \int_{E_{\mathrm{th}}}^{E_{\mathrm{e}}} \sigma(E)\Phi(E)\mathrm{d}E \Big/ \int_{E_{\mathrm{th}}}^{E_{\mathrm{e}}} \Phi(E)\mathrm{d}E, \qquad (1)$$

where $\sigma(E)$ is the reaction cross-section at photon energy E, $\Phi(E)$ is the photon flux, E_{e} is the electron energy, E_{th} is the photonuclear reaction threshold.

Using the bremsstrahlung driven by laser-plasma-accelerated electron beams described in Sect. II, we conducted experimental measurements on the (γ,xn) cross sections of ^{197}Au and compared them against the theoretical estimations based on Eq. 1. The experimental details and data analysis can be found in Ref. [73]. The agreement between experimental results and theory was found, which demonstrates that the procedure of measuring FACS with laser-driven bremsstrahlung is feasible. With this premise, we further evaluated the expected FACS of possible isomer residuals when laser-driven bremsstrahlung beams were used for the photoactivation of ^{197}Au, ^{180}Hf, ^{159}Tb, ^{115}In, ^{103}Rh, and ^{90}Zr, as shown in Fig. 5. Noticeably, for the FACS to produce the nuclear isomers ^{196m1}Au, ^{195m}Au, ^{179m1}Hf, ^{158m}Tb, ^{114m}In, ^{101m}Rh, and ^{89m}Zr were relatively larger than the others, exceeding the value of 10 mb. Moreover, the available experimental FACS to produce nuclear isomers for these target nuclei is very limited. The evaluated FACS for the production of ^{196m2}Au from the (γ, n) reaction on ^{197}Au agrees well with the experimental measurements made by Naik *et al*. [61], while those for the production of ^{102m,101m,100m,99m}Rh produced from (γ,xn) reactions on ^{103}Rh are all lower than the experimental values obtained by Rahman et al. [62]. The FACS for the isomers of the other isotopes produced from reactions, such as (γ, p) and (γ, α) reactions are also shown in the Supplementary Material, which are less abundant in the experimental data. These results show that experimental efforts to measure FACS involving isomer residuals are expected to resolve discrepancies and deficiencies in photonuclear data in the QD region.

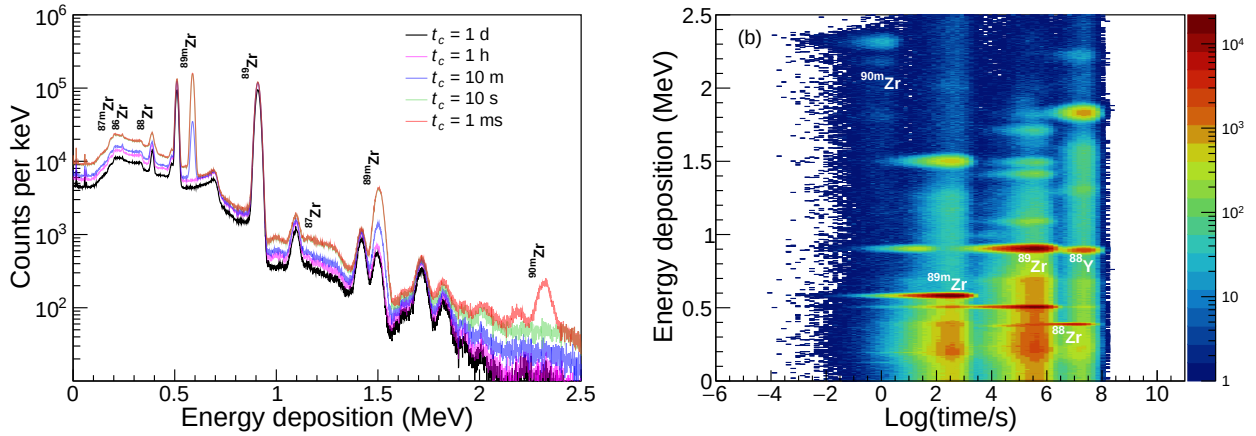

Fig. 7. (Color online) (a) The recorded γ-ray spectra for the photonuclear products of ^{90}Zr when the cooling time t_c is 1 ms, 10 s, 10 m, 1 h, and 1 d. The data acquisition time is set to 14 days. Here the offline detection of delayed radiation is imitated by applying a time window for the energy deposition in the detector. (b) The dependence of recorded counts on the energy deposition and detection time.

B. Dependence of isomer ratio on nuclear structure ingredients

The ratio of the probabilities of forming the isomer and the ground state is called the isomeric ratio, which can be given by:

$$IR_{\mathrm{m}i/\mathrm{g}} = \frac{\sigma^{\mathrm{m}i}_{\mathrm{FA}}(E_{\mathrm{e}})}{\sigma^{\mathrm{g}}_{\mathrm{FA}}(E_{\mathrm{e}})} = \frac{\int_{E'_{\mathrm{th}}}^{E_{\mathrm{e}}} \sigma_{\mathrm{m}i}(E)\Phi(E)\mathrm{d}E \,/\, \int_{E'_{\mathrm{th}}}^{E_{\mathrm{e}}} \Phi(E)\mathrm{d}E}{\int_{E_{\mathrm{th}}}^{E_{\mathrm{e}}} \sigma_{\mathrm{g}}(E)\Phi(E)\mathrm{d}E \,/\, \int_{E_{\mathrm{th}}}^{E_{\mathrm{e}}} \Phi(E)\mathrm{d}E} \quad (2)$$

where $\sigma^{\mathrm{m}i}_{\mathrm{FA}}(E_{\mathrm{e}})$ and $\sigma^{\mathrm{g}}_{\mathrm{FA}}(E_{\mathrm{e}})$ are the FACS to produce the i-th isomer and ground state, respectively. $\sigma_{\mathrm{m}i}(E)$ and $\sigma_{\mathrm{g}}(E)$ are the production cross-sections for the i-th isomer and ground state, respectively. The production threshold for the ith isomer E'_{th} differs slightly from that for the ground state E_{th}. In this study, we theoretically investigated the sensitivity of IR to three nuclear structure ingredients, including NLD, OMP, and SF. In particular, the IRs of $^{196\mathrm{m}2}$Au to $^{196\mathrm{g}}$Au ($\mathrm{IR}_{\mathrm{m2/g}}$), $^{196\mathrm{m}1}$Au to $^{196\mathrm{g}}$Au ($\mathrm{IR}_{\mathrm{m1/g}}$), and $^{196\mathrm{m}2}$Au to the sum of $^{196\mathrm{g}}$Au and $^{196\mathrm{m}1}$Au ($\mathrm{IR}_{\mathrm{m2/(m1+g)}}$) produced from the ($\gamma$, n) reactions of Au are evaluated using different sets of NLDs, OMPs, and SFs available in TALYS.

The results are predicted using six sets of NLDs (1 - Constant temperature Fermi gas model [74], 2 - Back-shifted Fermi gas model [75], 3 - Generalised superfluid model [76], 4 - HFB-Skyrme model [77], 5 - HFB-Skyrme model with combinatorial method [78], and 6 - Temperature(T)-dependent HFB-Gogny model [79]), two sets of OMPs (0 - phenomenological Wood-Saxon potential [80], 1 - semi-microscopic JLMB potential with HFB-Skyrme matter density [68, 81–83]), and eight sets of PSFs (1 - Generalized Lorentzian [84], 2 - Brink-Axel Lorentzian [85, 86], 3 - HFBCS-QRPA model [87], 4 - HFB-Skyrme-QRPA model [88], 5 - Hybrid model [89], 6 - T-dependent HFB-Skyrme-QRPA model [88, 90], 7 - T-dependent RMF model [91], and 8 - HFB-D1M-QRPA model [92]) are shown in Fig. 6. It is shown that the IRs grow rapidly with the increase in incident electron energy at low energies and tend to saturate at great energies of tens to hundreds MeV, where discrepancies resulting from different models occur. Specifically, $\mathrm{IR}_{\mathrm{m1/g}}$ is not sensitive to the three nuclear ingredients, whereas both $\mathrm{IR}_{\mathrm{m2/(m1+g)}}$ and $\mathrm{IR}_{\mathrm{m2/g}}$ show relatively strong sensitivity to the SFs and NLDs. This suggests that the existing experimental data and further measurements aimed at IRs, especially in high-energy regions, can be used to constrain these nuclear-structure ingredients.

V. DETECTION OF CHARACTERISTIC DECAYS

In photonuclear experiments, there are two ways to measure the reaction cross-sections: online detection of photo-induced particle emissions (neutrons, protons, and α particles) and offline detection of the characteristic γ decays of radioactive residuals. The former is generally used in experiments conducted with energy-tunable, quasi-monochromatic probes, such as laser-Compton γ-ray sources and positron annihilation in flight because the energy spectra of the emitted particles would exhibit easily identifiable reaction kinematics. In bremsstrahlung-driven photonuclear experiments, offline detection is typically performed. The detection of residuals depends not only on their decay characteristics and production yields but also on the energy resolution of the detector.

We performed Geant4 simulations to evaluate the feasibility of detecting the considered isomers produced in photonuclear reactions. The simulation setup is arranged as follows. The energy distribution and angular spread of the bremmstrahlung produced by the LWFA electrons are set according to the experimental results obtained at a gas pressure of 36 bar. The electron charge was set as 100 shots at 300 pC. The bremsstrahlung photons irradiated the activation targets with a thickness of 5 mm, placed 20 cm downstream of the converter, inducing photonuclear reactions and producing ra-

Table 1. The expected counts, half-lives, γ-ray energies, and intensities of the principal decays from the photonuclear products of ^{197}Au, ^{180}Hf, ^{159}Tb, ^{115}In, ^{103}Rh, and ^{90}Zr. The cooling time t_c is assumed as 1 μs. The data acquisition time is set as 14 days. The level energy of ^{195m2}Au is labeled as 2460.84+X keV because its transition energy to the level at 2460.84 keV is not determined yet.

Isotope	Half-life	Level energy (keV)	Decay energy (keV)	Intensity (%)	Net counts (14 d)
^{197m}Au	7.73 s	409.16	279.01	70.9	5.94×10^4
^{196}Au	6.1669 d	0.00	355.73	87	4.44×10^6
^{196m1}Au	8.1 s	84.66	9.71	25	N/A
^{196m2}Au	9.6 h	595.66	147.81	43.5	2.02×10^2
^{195}Au	186.01 d	0.00	98.86	11.21	4.03×10^2
^{195m1}Au	30.5 s	318.60	261.75	68.7	1.69×10^5
^{195m2}Au	12.89 μs	2460.84+X	X	N/A	N/A
^{194}Au	38.02 h	0.00	328.46	60.4	1.23×10^5
^{194m1}Au	600 ms	107.40	45.32	5.4	N/A
^{194m2}Au	420 ms	475.80	170.78	27.3	2.22×10^2
^{193}Au	17.65 h	0.00	255.57	6.5	3.52×10^3
^{193m}Au	3.9 s	209.203	257.97	67.14	2.22×10^4
^{180m}Hf	5.53 h	1141.50	332.27	94.00	N/A
^{179m1}Hf	18.67 s	375.00	214.34	95.3	1.29×10^6
^{179m2}Hf	25.05 d	1105.70	453.59	68	2.77×10^3
^{178m1}Hf	4 s	1147.40	426.36	97	1.73×10^4
^{178m2}Hf	31 y	2446.10	574.22	88.6	7.25×10^2
^{177m1}Hf	1.09 s	1315.50	208.37	73.1	1.24×10^3
^{177m2}Hf	51.4 m	2740.00	277.30	75	4.42×10^2
^{158}Tb	180 y	0.00	944.19	44.40	5.65×10^2
^{158m1}Tb	10.7 s	110.30	110.30	0.92	1.37×10^3
^{158m2}Tb	0.40 ms	388.40	171.07	50.4	2.76×10^3
^{157}Tb	71 y	0.00	54.50	0.0084	N/A
^{156}Tb	5.35 d	0.00	199.19	67	6.35×10^3
^{156m1}Tb	24.4 h	49.60	49.63	74.1	N/A
^{156m2}Tb	5.3 h	88.40	88.40	1.15	8.59×10^2
^{155}Tb	5.32 d	0.00	105.32	25.1	4.02×10^2
^{115m}In	4.486 h	336.20	336.24	45.90	1.59×10^5
^{114}In	71.9 s	0.00	1299.83	0.14	2.43×10^3
^{114m1}In	49.51 d	190.30	725.24	4.4	2.66×10^4
^{114m2}In	43.1 ms	501.95	311.65	89.85	1.05×10^6
^{113m}In	99.476 m	391.70	391.70	64.94	1.68×10^5
^{112}In	14.88 m	0.00	617.52	1	9.92×10^3
^{112m1}In	20.67 m	156.60	156.61	13.33	1.15×10^4
^{112m2}In	2.81 μs	613.82	187.93	N/A	1.13×10^4
^{111}In	2.8047 h	0.00	245.35	94.1	7.20×10^4
^{111m}In	7.7 m	537.00	537.00	87	9.99×10^3
^{103m}Rh	56.114 m	39.80	39.76	0.07	N/A
^{102}Rh	207.3 d	0.00	475.06	46	1.57×10^5
^{102m}Rh	3.742 y	140.70	697.49	44	1.18×10^3
^{101}Rh	3.3 y	0.00	198.01	73	5.60×10^3
^{101m}Rh	4.34 d	157.30	306.86	81	9.21×10^5
^{100}Rh	20.8 h	0.00	539.51	80.6	2.91×10^5
^{100m}Rh	4.6 m	107.60	539.60	1.68	2.91×10^5
^{99}Rh	16.1 d	0.00	528.24	37.9	1.58×10^4
^{99m}Rh	4.7 h	64.60	340.80	72	4.80×10^4
^{90m}Zr	809.2 ms	2319.00	2318.96	83.00	1.28×10^4
^{89}Zr	78.41 h	0.00	909.15	99.04	3.37×10^6
^{89m}Zr	4.161 m	587.80	1507.40	6.06	1.43×10^5
^{88}Zr	83.4 d	0.00	392.87	97.29	5.20×10^4
^{87}Zr	1.68 h	0.00	1227.00	2.8	5.03×10^2
^{87m}Zr	14 s	335.80	201.02	96.4	6.32×10^3
^{86}Zr	16.5 h	0.00	242.80	95.84	1.38×10^4

dioactive residuals. The γ decays of the radioactive residuals, including the isomers, were recorded by a $LaBr_3$ detector with dimensions of ϕ 8 cm $\times$ 10 cm assembled at 90° with respect to the beam propagation. The energy resolution is set as 3%, which is achievable for commercially available $LaBr_3$ detectors. To simulate isomer production and decay radiation detection in a one-stop manner, we adopted the Geant4-GENBOD [30–32] toolkit and further implemented the radioactive decay process of the radioactive residuals (including the isomers). The photonuclear reaction cross-sections of the related isotopes were calculated with a routine similar to Sect. III B.

An exemplary correlation of energy deposition versus detection time for the radioactive residuals induced by photonuclear reactions on ^{90}Zr is given in Fig. 7. In activation experiments based on laser-plasma acceleration, there is a period (cooling time t_c) for opening the reaction chamber before the activated samples are handed to the detector for data acquisition. If t_c is larger than 1 h and 10 s, the decay information of the products ^{89m}Zr ($T_{1/2}$ = 4.16 m) and ^{90m}Zr ($T_{1/2}$ = 809 ms) will be lost. To detect isomers with short half-lives, such as ^{90m}Zr the detector is placed near the activation target in an "online" manner. The backgrounds induced by the backscattered bremsstrahlung, electrons, and electromagnetic pulses can be cut off by applying a time window with a delay signal generator. The correlation of energy deposition versus detection time for the radioactive residuals induced by the photonuclear reactions on all six selected targets is presented in the Supplementary Material. The principal decay characteristics and expected counts within three half-lives for the isomers produced from the photonuclear reactions of the six selected isotopes are shown in Table 1. The photonuclear products ^{196m1}Au, ^{194m1}Au, ^{157}Tb, ^{156m1}Tb, and ^{103m}Rh are not measurable for the $LaBr_3$ detector because their decay energy is too little and the attenuation in the target is strong. The measurement of ^{195m2}Au is unlikely because its decay energy and intensity has not yet been determined. For ^{180}Hf, the decay of ^{180m}Hf is difficult to measure because the (γ, γ') reaction cross-section is very low. In addition, most of the isomer residuals can be measured with a net count of 10^{2-6} within 14 days of data acquisition. The decay energies of some products, such as ^{193}Au and ^{193m}Au are very close and cannot be disentangled from the recorded energy spectrum of a detector with poor energy resolution. However, this can be remedied by applying a fit to the recorded counts in a few data-acquisition cycles.

VI. CONCLUSION

In this study, we calculated the production cross-sections of nuclear isomers from the photonuclear reaction on ^{197}Au, ^{180}Hf, ^{159}Tb, ^{115}In, ^{103}Rh, and ^{90}Zr with TALYS. Deficiencies in the corresponding experimental data were found in the comparison between theoretical estimations and the available data from EXFOR. Laser-plasma electron acceleration experiments carried out at CLAPA are introduced. Stable LWFA electrons with energies of 78 $\pm$ 10, 103 $\pm$ 14, and 135 $\pm$ 20 MeV can be obtained with a charge of 300 $-$ 600 pC per shot. The resulting peak bremsstrahlung flux is expected to be 1.24 $\times$ 10^{19} photons/s. To evaluate the prospect of using such a photon beam for photonuclear studies regarding nuclear isomers, the FACSs and IRs for isomer production were deduced and, compared with the data found in EXFOR. The sensitivity of IRs against the nuclear ingredients SF and NLD was determined, which highlights the importance of measuring photonuclear reactions involving isomers. Moreover, the prospect of photonuclear measurement of nuclear isomers using LWFA electrons at CLAPA is foreseen with Geant4 simulations.

VII. ACKNOWLEDGEMENT

The authors thank the staff of the 200 TW laser of CLAPA laboratory for the smooth operation of the machine.

AUTHOR CONTRIBUTIONS

All authors contributed to the study conception and design. Material preparation, data collection, and analysis were performed by Hao-Yang Lan, Di Wu, Jia-Xin Liu, Jian-Yao Zhang, Huan-Gang Lu, Jian-Feng Lv and Xue-Zhi Wu. The first draft of the manuscript was written by Hao-Yang Lan and all authors commented on previous versions of the manuscript. All authors read and approved the final manuscript.

DATA AVAILABILITY STATEMENT

The data that support the findings of this study are openly available in Science Data Bank at https://doi.org/10.57760/sciencedb.j00186.00066 and https://cstr.cn/31253.11.sciencedb.j00186.00066.

[1] F. Soddy, The stability of lead isotopes from thorium. Nature **99**, 244–245 (1917). 10.1038/099244c0
[2] O. Hahn, Über ein neues radioaktives zerfallsprodukt im uran. Naturwissenschaften **9**, 84–84 (1921). 10.1007/BF01491321
[3] P. Walker and Z. Podolyák, 100 years of nuclear isomers—then and now. Phys. Scr. **95**, 044004 (2020). 10.1088/1402-4896/ab635d
[4] A. K. Jain, B. Maheshwari, A. Goel, *Nuclear Isomers: A Primer*. Springer Nature (2021).
[5] C. Chiara, J. Carroll, M. Carpenter et al, Isomer depletion as experimental evidence of nuclear excitation by electron capture. Nature **554**, 216–218 (2018). 10.1038/nature25483

[6] J. Gunst, Y. A. Litvinov, C. H. Keitel et al, Dominant secondary nuclear photoexcitation with the X-ray free-electron laser. Phys. Rev. Lett. **112**, 082501 (2014). 10.1103/PhysRevLett.112.082501

[7] J. Thielking, M. V. Okhapkin, P. Głowacki et al, Laser spectroscopic characterization of the nuclear-clock isomer ^{229m}Th. Nature **556**, 321–325 (2018). 10.1038/s41586-018-0011-8

[8] S. Guo, B. Ding, X. H. Zhou et al, Probing ^{93m}Mo isomer depletion with an isomer beam. Phys. Rev. Lett. **128**, 242502 (2022). 10.1103/PhysRevLett.128.242502

[9] Y. Wu, C. H. Keitel, A. Pálffy, ^{93m}Mo isomer depletion via beam-based nuclear excitation by electron capture. Phys. Rev. Lett. **122**, 212501 (2019). 10.1103/PhysRevLett.122.212501

[10] G. Lotay, A. Lennarz, C. Ruiz et al., Radiative capture on nuclear isomers: Direct measurement of the ^{26m}Al(p,γ)^{27}Si reaction. Phys. Rev. Lett. **128**, 042701 (2022). 10.1103/PhysRevLett.128.042701

[11] T. Tajima and J. M. Dawson, Laser electron accelerator. Phys. Rev. Lett. **43**, 267 (1979). 10.1103/PhysRevLett.43.267.

[12] J. Faure, Y. Glinec, A. Pukhov et al., A laser–plasma accelerator producing monoenergetic electron beams. Nature **431**, 541–544 (2004). 10.1038/nature02963

[13] C. Geddes, C. Toth, J. Van Tilborg et al., High-quality electron beams from a laser wakefield accelerator using plasma-channel guiding. Nature **431**, 538–541 (2004). 10.1038/nature02900.

[14] S. P. Mangles, C. Murphy, Z. Najmudin et al., Monoenergetic beams of relativistic electrons from intense laser–plasma interactions. Nature **431**, 535–538 (2004). 10.1038/nature02939.

[15] A. Modena, Z. Najmudin, A. Dangor et al., Electron acceleration from the breaking of relativistic plasma waves. Nature **377**, 606–608 (1995). 10.1038/377606a0.

[16] A. Pukhov and J. Meyer-ter Vehn, Laser wake field acceleration: the highly non-linear broken-wave regime. Appl. Phys. B **74**, 355–361 (2002). 10.1007/s003400200795.

[17] W. Lu, C. Huang, M. Zhou et al., Nonlinear theory for relativistic plasma wakefields in the blowout regime. Phys. Rev. Lett. **96**, 165002 (2006). 10.1103/PhysRevLett.96.165002.

[18] V.G. Nedorezov, S.G. Rykovanov, A.B. Savel'ev, Nuclear photonics: results and prospects. PHYS-USP+ **64**, 1214 (2021). 10.3367/UFNe.2021.03.038960.

[19] J. Feng, W.Z. Wang, C.B. Fu et al., Femtosecond pumping of nuclear isomeric states by the coulomb collision of ions with quivering electrons. Phys. Rev. Lett. **128**, 052501 (2022). 10.1103/PhysRevLett.128.052501.

[20] W. Wang, J. Zhou, B.Q. Liu et al., Exciting the isomeric ^{229}Th nuclear state via laser-driven electron recollision. Phys. Rev. Lett. **127**, 052501 (2021). 10.1103/PhysRevLett.127.052501

[21] Z.G. Ma, C.B. Fu, W.B. He et al., Manipulation of nuclear isomers with lasers: mechanisms and prospects. Sci. Bull. **67**, 1526–1529 (2022). 10.1016/j.scib.2022.06.020

[22] W. T. Pan, T. Song, H.Y. Lan et al., Photo-excitation production of medically interesting isomers using intense γ-ray source. Appl. Radiat. Isot. **168**, 109534 (2021). 10.1016/j.apradiso.2020.109534

[23] I. Spencer, K. Ledingham, R. Singhal et al., A nearly real-time high temperature laser–plasma diagnostic using photonuclear reactions in tantalum. Rev. Sci. Instrum. **73**, 3801–3805 (2002). 10.1063/1.1511802.

[24] X.L. Wang, Z.C. Xu, W. Luo et al., Transmutation prospect of long-lived nuclear waste induced by high-charge electron beam from laser plasma accelerator. Phys. Plasmas **24**, 093105 (2017). 10.1063/1.4998470.

[25] Z.G. Ma, H.Y. Lan, W.Y. Liu, Photonuclear production of medical isotopes ^{62,64}Cu using intense laser-plasma electron source. Matter Radiat. at Extremes **4**, 064401 (2019). 10.1063/1.5100925

[26] S. Agostinelli, J. Allison, K. a. Amako, et al. GEANT4 - a simulation toolkit. Nucl. Instrum. Methods Phys. Res. A **506**, 250–303 (2003). 10.1016/S0168-9002(03)01368-8.

[27] A. Koning, D. Rochman, J. C. Sublet et al., TENDL: Complete nuclear data library for innovative nuclear science and technology. Nucl. Data Sheets **155**, 1–55 (2019). 10.1016/j.nds.2019.01.002

[28] E. Alhassan, D. Rochman, A. Vasiliev et al., Iterative Bayesian Monte Carlo for nuclear data evaluation. Nucl. Sci. Tech. **33**, 50 (2022). 10.1007/s41365-022-01034-w

[29] N. Otuka, E. Dupont, V. Semkova et al., Towards a more complete and accurate experimental nuclear reaction data library (EXFOR): international collaboration between nuclear reaction data centres (NRDC). Nucl. Data Sheets **120**, 272–276 (2014), 10.1016/j.nds.2014.07.065

[30] W. Luo, H. Y. Lan, Y. Xu et al., Implementation of the n-body Monte-Carlo event generator into the Geant4 toolkit for photonuclear studies. Nucl. Instrum. Methods Phys. Res. A **849**, 49–54 (2017). 10.1016/j.nima.2017.01.010

[31] H.Y. Lan, Y. Xu, W. Luo et al., Determination of the photodisintegration reaction rates involving charged particles: Systematic calculations and proposed measurements based on the facility for Extreme Light Infrastructure–Nuclear Physics. Phys. Rev. C **98**, 054601 (2018). 10.1103/PhysRevC.98.054601

[32] H. Y. Lan, W. Luo, Y. Xu et al., Feasibility of studying astrophysically important charged-particle emission with the variable energy γ-ray system at the Extreme Light Infrastructure–Nuclear Physics facility. Phys. Rev. C **105**, 044618 (2022). 10.1103/PhysRevC.105.044618

[33] K. Vogt, P. Mohr, M. Babilon et al., Measurement of the (γ, n) cross section of the nucleus ^{197}au close above the reaction threshold. Nucl. Phys. A **707**, 241–252 (2002). 10.1016/S0375-9474(02)00922-3

[34] C. Plaisir, F. Hannachi, F. Gobet et al., Measurement of the ^{85}Rb(γ, n)^{84m}Rb cross-section in the energy range 10-19 MeV with bremsstrahlung photons. Eur. Phys. J. A **48**, 1–5 (2012). 10.1140/epja/i2012-12068-7

[35] A. Goryachev and G. Zalesnyi, Giant dipole resonance in Hf isotopes. Sov. J. Nucl. Phys.(Engl. Transl.);(United States) **26** (1977).

[36] B. Goryachev, Y. Kuznetsov, V. Orlin, et al. Giant resonance in the strongly deformed nuclei ^{159}Tb, ^{165}Ho, ^{166}Er, and ^{178}Hf. Sov. J. Nucl. Phys.(Engl. Transl.);(United States) **23** (1976).

[37] O. Bogdankevich, B. Goryachev, and V. Zapevalov, Splitting of the giant resonance in medium-heavy nuclei. Zhur. Eksptl'. i Teoret. Fiz. **42** (1962).

[38] R. Parsons, The photodisintegration of manganese and rhodium. Can. J. Phys. **37**, 1344–1348 (1959). 10.1139/p59-154.

[39] D. Brajnik, D. Jamnik, G. Kernel et al., Photonuclear reactions in ^{90}Zr. Phys. Rev. C **13**, 1852–1863 (1976). 10.1103/PhysRevC.13.1852

[40] K. Y. Hara, H. Harada, F. Kitatani et al., Measurements of the ^{152}Sn (γ, n) cross-section with laser-Compton scattering γ rays and the photon difference method. J. Nucl. Sci. Technol. **44**, 938–945 (2007). 10.1080/18811248.2007.9711333

[41] O. Itoh, H. Utsunomiya, H. Akimune et al., Photoneutron cross sections for Au revisited: measurements with laser Compton scattering γ-rays and data reduction by a least-

squares method. J. Nucl. Sci. Technol. **48**, 834–840 (2011). 10.1080/18811248.2011.9711766

[42] F. Kitatani, H. Harada, S. Goko et al., Measurement of the ^{80}Se (γ, n) cross section using laser-Compton scattering γ-rays. J. Nucl. Sci. Technol. **47**, 367–375 (2010). 10.1080/18811248.2010.9711967

[43] F. Kitatani, H. Harada, S. Goko et al., Measurement of ^{76}Se and ^{78}Se (γ, n) cross sections. J. Nucl. Sci. Technol. **48**, 1017–1024 (2011). 10.1080/18811248.2011.9711787

[44] A. Banu, E. G. Meekins, J. A. Silano et al., Photoneutron reaction cross section measurements on ^{94}Mo and ^{90}Zr relevant to the *p*-process nucleosynthesis. Phys. Rev. C **99**, 025802 (2019). 10.1103/PhysRevC.99.025802

[45] B.L. Berman, R.E. Pywell, S.S. Dietrich et al., Absolute photoneutron cross sections for Zr, I, Pr, Au, and Pb. Phys. Rev. C **36**, 1286–1292 (1987). 10.1103/PhysRevC.36.1286

[46] A. Veyssiere, H. Beil, R. Bergere et al., Photoneutron cross sections of ^{208}Pb and ^{197}Au. Nucl. Phys. A **159**, 561–576 (1970). 10.1016/0375-9474(70)90727-X

[47] S.C. Fultz, R.L. Bramblett, J.T. Caldwell et al., Photoneutron cross-section measurements on gold using nearly monochromatic photons. Phys. Rev. **127**, 1273–1279 (1962). 10.1103/PhysRev.127.1273

[48] R. Bergere, H. Beil, A. Veyssiere, Photoneutron cross sections of La, Tb, Ho and Ta. Nucl. Phys. A **121**, 463–480 (1968). 10.1016/0375-9474(68)90433-8

[49] R.L. Bramblett, J.T. Caldwell, R.R. Harvey et al., Photoneutron cross sections of Tb^{159} and O^{16}. Phys. Rev. **133**, B869–B873 (1964). 10.1103/PhysRev.133.B869

[50] A. Lepretre, H. Beil, R. Bergere et al., A study of the giant dipole resonance of vibrational nuclei in the $103 \leq A \leq 133$ mass region. Nucl. Phys. A **219**, 39–60 (1974). 10.1016/0375-9474(74)90081-5

[51] S.C. Fultz, B.L. Berman, J.T. Caldwell et al., Photoneutron cross sections for Sn^{116}, Sn^{117}, Sn^{118}, Sn^{119}, Sn^{120}, Sn^{124}, and indium. Phys. Rev. **186**, 1255–1270 (1969). 10.1103/PhysRev.186.1255

[52] A. Lepretre, H. Beil, R. Bergere et al., The giant dipole states in the A = 90 mass region. Nucl. Phys. A **175**, 609–628 (1971). 10.1016/0375-9474(71)90454-4.

[53] B.L. Berman, J.T. Caldwell, R.R. Harvey et al., Photoneutron cross sections for Zr^{90}, Zr^{91}, Zr^{92}, Zr^{94}, and Y^{89}. Phys. Rev. **162**, 1098–1111 (1967). 10.1103/PhysRev.162.1098

[54] V. Bokhinyuk, A. Guthy, A. Parlag et al., Study of the effective excitation cross section of the ^{115}In isomeric state in the (gamma, gamma') reaction. Ukrayins' kij Fyizichnij Zhurnal (Kiev) **51**, 657–660 (2006).

[55] W. Tornow, M. Bhike, S. W. Finch et al., Measurement of the ^{115}In (γ, γ') ^{115m}In inelastic scattering cross section in the 1.8 to 3.7 MeV energy range with monoenergetic photon beams. Phys. Rev. C **98**, 064305 (2018). 10.1103/PhysRevC.98.064305

[56] V. M. Mazur, I. V. Sokolyuk, Z. M. Bigan et al., Cross section for excitation of nuclear isomers in (γ,γ')(m) reactions at 4-15 MeV. Yadernaya Fizika **56**, 20 (1993).

[57] N.A. Demekhina, A.S. Danagulyan, G.S. Karapetyan, Formation of isomeric states in (γ,γ') reactions at energies around the Giant Dipole Resonance. Yadernaya Fizika **64**, 1879 (2001). 10.1134/1.1414927

[58] O. Bogdankevich, L. Lazareva, F. Nikolaev, Inelastic scattering of photons by indium-115 nuclei. Soviet Phys. JETP **4** (1957).

[59] N. Mutsuro, Y. Ohnuki, K. Sato et al., Photoneutron cross sections for Ag^{107}, Mo^{92} and Zr^{90}. J. Phys. Soc. Japan **14**, 1649 (1959). 10.1143/JPSJ.14.1649

[60] D. Brajnik, D. Jamnik, G. Kernel et al., Photonuclear reactions in ^{90}Zr. Phys. Rev. C **13**, 1852 (1976). 10.1103/PhysRevC.13.1852

[61] H. Naik, G. Kim, K. Kim et al., Measurement of flux-weighted average cross sections for ^{197}Au (γ, xn) reactions and isomeric yield ratios of ^{196m,g}Au with bremsstrahlung. Nucl. Phys. A **948**, 28–45 (2016). 10.1016/j.nuclphysa.2016.01.015

[62] S. Rahman, K. Kim, G. Kim et al., Measurement of flux-weighted average cross-sections and isomeric yield ratios for ^{103}Rh (*gamma*, xn) reactions in the bremsstrahlung end-point energies of 55 and 60 MeV. Eur. Phys. J. A **52**, 1–12 (2016). 10.1140/epja/i2016-16194-x

[63] I. N. Vishnevsky, V. A. Zheltonozhsky, I. N. Kadenko et al., Isomeric ratios of (γ,p) and (γ,α) reactions on ^{117m,g}In. Bull. Russ. Acad. Sci. Phys. **72**, 1569 (2008). 10.3103/S1062873808110294

[64] S. R. Palvanov and O. Razhabov, Isomer yield ratios of photonuclear reactions at $E_{\gamma max}$ 25 and 30 MeV. Atomnaya Energiya **87**, 75 (1999).

[65] M. S. Rahman, K. S. Kim, M. Lee et al., Measurement of isomeric-yield ratios for the ^{197}Au(γ,n)^{196m,g}Au reactions induced by bremsstrahlung. J. Radioanal. Nucl. Chem. **283**, 519 (2010). 10.1007/s10967-009-0375-1

[66] T.D. Thiep, T.T. An, N.T. Vinh et al., Experimental study and theoretical consideration of the isomeric ratio in photonuclear reaction ^{197}Au(γ,n)^{196m,g}Au in the giant dipole resonance region. Phys. Part. Nucl. Lett. **3**, 223 (2006). 10.1134/S1547477106040017

[67] W.J. Huang, G. Audi, M. Wang et al., The AME2016 atomic mass evaluation (I). Evaluation of input data and adjustment procedures. Chin. Phys. C **41**, 030002 (2017). 10.1088/1674-1137/41/3/030002

[68] S. Goriely, N. Chamel, J. M. Pearson, Hartree-Fock-Bogoliubov nuclear mass model with 0.50 MeV accuracy based on standard forms of Skyrme and pairing functionals. Phys. Rev. C **88**, 061302 (2013). 10.1103/PhysRevC.88.061302

[69] R. Capote, M. Herman, P. Obložinskỳ et al., RIPL–reference input parameter library for calculation of nuclear reactions and nuclear data evaluations. Nucl. Data Sheets **110**, 3107–3214 (2009). 10.1016/j.nds.2009.10.004

[70] K. Tanaka, K. Spohr, D. Balabanski et al., Current status and highlights of the ELI-NP research program. Matter Radiat. at Extremes **5**, 024402 (2020). 10.1063/1.5093535

[71] H.W. Wang, G.T. Fan, L.X. Liu et al., Commissioning of laser electron gamma beamline SLEGS at SSRF. Nucl. Sci. Tech. **33**, 1–12 (2022). 10.1007/s41365-022-01076-0

[72] G. P. An, Y. L. Chi, Y. L. Dang et al., High energy and high brightness laser Compton backscattering gamma-ray source at IHEP. Matter Radiat. Extremes **3**, 219–226 (2018). 10.1016/j.mre.2018.01.005

[73] D. Wu, J. Y. Zhang, H. Y. Lan et al., ^{197}Au(γ, xn; x = 1-7) reaction measurements using laser-driven ultra-bright ultra-fast bremsstrahlung γ-ray. arXiv:2209.13947 (2022). 10.48550/arXiv.2209.13947

[74] A. Gilbert and A. G. W. Cameron, A composite nuclear-level density formula with shell corrections. Can. J. Phys. **43**, 1446 (1965). 10.1139/p65-139

[75] W. Dilg, W. Schantl, H. Vonach et al., Level density parameters for the back-shifted Fermi gas model in the mass range $40 < A < 250$. Nucl. Phys. A **217**, 269–298 (1973). 10.1016/0375-9474(73)90196-6.

[76] A.V. Ignatyuk, J.L. Weil, S. Raman et al., Density of discrete levels in ^{116}Sn. Phys. Rev. C **47**, 1504–1513 (1993). 10.1103/PhysRevC.47.1504

[77] S. Goriely, F. Tondeur, J. Pearson, A Hartree-Fock nuclear mass table. At. Data Nucl. Data Tables **77**, 311–381 (2001). , https://doi.org/10.1006/adnd.2000.0857.

[78] S. Goriely, S. Hilaire, A.J. Koning, Improved microscopic nuclear level densities within the Hartree-Fock-Bogoliubov plus combinatorial method. Phys. Rev. C **78**, 064307 (2008). 10.1103/PhysRevC.78.064307

[79] S. Hilaire, M. Girod, S. Goriely et al., Temperature-dependent combinatorial level densities with the D1M Gogny force. Phys. Rev. C **86**, 064317 (2012). 10.1103/PhysRevC.86.064317

[80] A. Koning and J. Delaroche, Local and global nucleon optical models from 1 keV to 200 MeV. Nucl. Phys. A **713**, 231–310 (2003). 10.1016/S0375-9474(02)01321-0

[81] J. P. Jeukenne, A. Lejeune, C. Mahaux, Many-body theory of nuclear matter. Phys. Rep. **25**, 83–174 (1976). 10.1016/0370-1573(76)90017-X

[82] J. P. Jeukenne, A. Lejeune, C. Mahaux, Optical-model potential in finite nuclei from Reid's hard core interaction. Phys. Rev. C **16**, 80 (1977). 10.1103/PhysRevC.16.80

[83] E. Bauge, J. Delaroche, M. Girod, Semimicroscopic nucleon-nucleus spherical optical model for nuclei with A $>\sim$ 40 at energies up to 200 MeV. Phys. Rev. C **58**, 1118 (1998). 10.1103/PhysRevC.58.1118.

[84] J. Kopecky and M. Uhl, Test of gamma-ray strength functions in nuclear reaction model calculations. Phys. Rev. C **41**, 1941–1955 (1990). 10.1103/PhysRevC.41.1941.

[85] D. Brink, Individual particle and collective aspects of the nuclear photoeffect. Nucl. Phys. **4**, 215–220 (1957). 10.1016/0029-5582(87)90021-6.

[86] P. Axel, Electric dipole ground-state transition width strength function and 7-MeV photon interactions. Phys. Rev. **126**, 671–683 (1962). 10.1103/PhysRev.126.671

[87] S. Goriely and E. Khan, Large-scale QRPA calculation of E1-strength and its impact on the neutron capture cross section. Nucl. Phys. A **706**, 217–232 (2002). 10.1016/S0375-9474(02)00860-6.

[88] S. Goriely, E. Khan, and M. Samyn, Microscopic HFB + QRPA predictions of dipole strength for astrophysics applications. Nucl. Phys. A **739**, 331–352 (2004). 10.1016/j.nuclphysa.2004.04.105.

[89] S. Goriely, Radiative neutron captures by neutron-rich nuclei and the r-process nucleosynthesis. Phys. Lett. B **436**, 10–18 (1998). 10.1016/S0370-2693(98)00907-1.

[90] S. Hilaire, M. Girod, S. Goriely et al., Temperature-dependent combinatorial level densities with the D1M Gogny force. Phys. Rev. C **86**, 064317 (2012). 10.1103/PhysRevC.86.064317.

[91] I. Daoutidis and S. Goriely, Large-scale continuum random-phase approximation predictions of dipole strength for astrophysical applications. Phys. Rev. C **86**, 034328 (2012). 10.1103/PhysRevC.86.034328

[92] S. Goriely, S. Hilaire, S. Péru et al., Gogny-HFB+QRPA dipole strength function and its application to radiative nucleon capture cross section. Phys. Rev. C **98**, 014327 (2018). 10.1103/PhysRevC.98.014327